Digital image correlation techniques for measuring tyre-road interface parameters: Part 1 - Side-slip angle measurement on rough terrain

Theunis R. Botha* & P. Schalk Els

Department of Mechanical and Aeronautical Engineering,

University of Pretoria, co Lynnwood Road and Roper Street,

Pretoria, 0002, South Africa

* Corresponding author.

E-mail address: trbotha@tuks.co.za

Telephone: +27 12 420 3289

E-mail address:

trbotha@tuks.co.za (Theunis R. Botha)

schalk.els@up.ac.za (P. Schalk Els)

Abstract

This paper presents inexpensive methods whereby the vehicle side-slip angle can be measured accurately at low speeds on any terrain using cameras. Most commercial side-slip angle sensor systems and estimation techniques rely on smooth terrain and high vehicle speeds, typically above 20km/h, to provide accurate measurements. However, during certain in-situ tyre and vehicle testing on off-road conditions, the vehicle may be traveling at speeds slower than required for current sensors and estimation techniques to provide sufficiently accurate results. Terramechanics tests are typical case in point. Three algorithms capable of determining the side-slip angle from overlapping images are presented. The first is a simple fast planar method. The second is a more complex algorithm which can extract not only the side-slip angle but also its rotational velocities and scaled translational velocities. The last uses a calibrated stereo-rig to obtain all rotations and translational movement in world coordinates. The last two methods are aimed more at rough terrain applications, where the terrain induces motion components other than typical predominant yaw-plane motion. The study however found no discernible difference in measured side-slip angle of the methods. The system allows for accurate measurement at low and higher speeds depending on camera speed and lighting.

1. INTRODUCTION

The vehicle side-slip angle is an important measurement in the handling of vehicles. It can be used as a measure of the handling and stability of the vehicle. The side-slip angle can describe the over steer and under steer characteristics of a vehicle when measured on the front and rear axle of the vehicle. It can also be a measure of vehicle directional stability. Measurement of the sideslip angle is therefore important when performing high speed dynamic manoeuvres with vehicles.

The tyre side-slip angle is also of great importance when performing tyre modelling and evaluation. While the lateral tyre force generation is a complex phenomenon in which the deformation of the rubber during cornering is non-uniform across the contacts patch as illustrated by Fiala's mathematical formulation [1] of tyre force generation. It can be shown that the side-force generation of a tyre can be sufficiently described using the average side-slip angle of a tyre [1], [2]. Accurate measurement of the side-slip angle is therefore crucial in validating and characterizing tyre models. In many terramechanics tests the tyre tests are performed in a laboratory with a controlled environment [3], [4]. In these laboratory tests the side-slip angle can be controlled accurately, however, these test rigs are expensive and as such numerous tests are conducted in-situ with the vehicle traveling across the surface. In these situations the side-slip angle needs to be accurately measured. Since these tests are typically conducted at low speeds the estimation method is generally not applicable. Various stability and traction control algorithms can be improved if an online measurement of the side-slip angle is available and can be cheaply measured. The side-slip angle and its derivative offer more practical information about the vehicle stability compared to yaw rate for vehicle stability [5]. Chung and Yi [6] develop a side-slip angle based stability control scheme and shows overall improvement in vehicle performance.

In literature many studies concentrate on estimating the side-slip angle through other vehicle measurements. The side-slip angle is estimated using sensors such as accelerometers, rate gyroscopes and GPS [7], [8]. The main disadvantages of the estimation methods are that they rely on high dynamic situations such as high speed manoeuvres where sensor excitations are large in comparison to sensor noise. Additionally when considering off-road terrain the additional ground excitation may become too large rendering these methods unsuitable. While in off-road driving scenarios especially on deformable or very low friction terrains, such as mud, sand, loose gravel, ice and snow, the side-slip angle may become large when fully sliding and can also occur at much slower speeds as compared to hard roads.

A commercial side-slip angle measurement sensor, Kistler Correvit S-HR [9], is available which uses both Doppler Effect and an absolute measuring method. However, the sensor generally provides unreasonable accuracy below 15km/h and has a maximum measurable side-slip angle of ±20deg. The sensor is also developed for use on mainly on-road vehicles where there is very little vertical body motion and the vehicle mainly undergoes planar motion i.e. high speed driving on smooth roads. It will however be shown that vertical motion as well as roll can have an effect on the measured side-slip angle.

This paper proposes three techniques whereby the side-slip angle is measured using either a single camera facing the ground or a calibrated stereographical rig containing two cameras. The three techniques make use of Digital Image Correlation (DIC) as well as other imaging techniques to determine the side-slip angle. The first proposed method is a simplistic technique which is very computationally inexpensive but only measures image longitudinal and lateral velocities. The second technique is a more computationally expensive method which can measure all rotational and scaled translation velocities. The last technique makes use of a calibrated stereographical rig to determine all rotations and translations in real world coordinates. All methods can measure any degree of slip angle and can accurately measure slip angles at very low speeds.

2. DIGITAL IMAGE CORRELATION TECHNIQUE

Digital Image Correlation (DIC) is a method whereby optical methods are used to track changes in an image. The methods can be used to obtain a variety of measurements from displacements and velocities of particles to the strain of an object in an image [10]. There are numerous methods which can be used to perform DIC, however the underlying methodology remains the same. The techniques try to match regions in one image to regions in another effectively tracking these regions across images. Often these images make up a time sequence of images, I_t [t=0, 1,…, n], taken with a constant time difference apart. In strain based measurements the displacement field is computed across the whole image, however to simplify and speed up the DIC smaller key point regions can be tracked as opposed to the complete image.

In order to track a subset of regions in the image first requires the identification of regions in the image which are easily identifiable and therefore easy to track. A simplistic feature to track in imaging are so called corner or edge features. These are features which there is texture (change in pixel intensity) in at least two directions. This is generally achieved by taking the second derivative of the image intensity in various directions to obtain a form of Hessian matrix as:

$$\boldsymbol{Z} = \begin{bmatrix} \frac{d^2I}{dx^2} & \frac{d^2I}{dxdy} \\ \frac{d^2I}{dxdy} & \frac{d^2I}{dy^2} \end{bmatrix} \tag{1}$$

A region is found to be good to track if the smallest eigenvalue of $\boldsymbol{Z}$ is above a certain threshold [11]. These locations can be further enhanced by obtaining the location in a sub-pixel manner. These features can then be tracked from one image to the next to using optical flow techniques. One of the most widely used techniques used for sparse optical flow (small subsets of regions are tracked instead of the whole image) is the Lucas-Kanade optical flow algorithm [12]. The algorithm makes three assumptions on the motion in order to track corners. The first assumption is that of brightness constancy, this implies that the brightness of the feature or region being tracked is consistent from frame to frame. This assumption, even if invalid when shadows are generated, can be forced to be valid using adjustable lighting, sensor gain, adjustable aperture and image contrast adjustment in post processing. The second assumption is that the features motion is relatively small, this implies that the feature does not move much from frame to frame. This assumption would be the first to be found invalid, as the time steps between frames are often not as small as desired. The Lucas-Kanade algorithm tries to alleviate this problem by performing an iterative approach. This improves convergence as long as the initial step is close to the solution. However, often much larger motions are observed. To circumvent this problem a modification is introduced which performs the tracking over layers of scaled images. Each layer contains an increasing smaller image from the bottom to the top. Thus, each layer effectively reduces the feature motion in increasing magnitude. The algorithm is performed on the top (smallest image) and the solution is then used on the next layer down until the algorithm is applied to the bottom level which corresponds to the original image. In this way much larger motions between frames can be tracked. The third and final assumption is that a small windowed region around the corner exhibits the same motion as that of the corner. This assumption is valid concerning most surfaces which will be traversed. Even deformable surface such as sand and mud which might exhibit motion in larger regions will exhibit smaller regions whose motion can be considered consistent with the feature motion. These algorithms are implemented using the OpenCV [13] library in C++.

For these algorithm to be employed requires that the surface under consideration exhibits some texture which generates features that can be tracked. The surface thus requires features to be present which is required to be observable in an image based on a change in pixel brightness. Fortunately most surfaces which a vehicle will traverse contain texture created by different aggregates or particles in the surface. Even plain sand contains

different sized and coloured aggregates which create enough texture allowing the implementation of this method.

3. SLIP ANGLE MEASUREMENT ALGORITHMS

This section describes the three various algorithms used to measure the side-slip angle using the tracked features obtained using DIC.

3.1. SLIP ANGLE MEASURMENT USING EFFICIENT 2D PLANAR METHOD

After features have been tracked between frames these tracked features can be used to estimate the relative motion between frames provided the features are stationary and that any lens distortion is removed. The lens distortion is removed using a calibration surface containing a grid of points of which the relative positions are known. Multiple images of this calibration surface are taken from different positions and orientations. These calibrations surface points are used in an optimisation procedure to estimate the parameters of the lens distortion. The lens calibration procedure is performed using OpenCV.

The tracked features describe the re-projected relative motion of the camera over the road. Since the features lateral and longitudinal displacement are measured simultaneously the angle of the feature motion can be considered the camera direction of travel. Thus, if the camera is mounted such that the features move horizontally, or vertically, when the side-slip angle is zero then the angle the features move in is effectively the side-slip angle. This assumption holds if the feature motions contain purely lateral and longitudinal motion, thus, all features will travel in the same direction. On smooth roads this assumption is generally valid as the vehicle undergoes mostly planar motion. Figure 1 depicts the tracking of features from one frame to another over a concrete surface with the line trace showing the relative motion between the previous frame and the current frame. From this image it can be observed that most features seem to be travelling in the same direction with the same magnitude, however at least one tracked feature can be observed to be tracked incorrectly. The incorrect tracking of features presents a problem to the measuring of the travel direction. While the figure shows the majority of the features moving in the same direction, it could occur that numerous features be tracked incorrectly causing an error in the measurement. It is therefore necessary to employ a form of outlier rejection to remove any incorrectly tracked features. The first phase of outlier rejection is provided by the Lucas-Kanade algorithm implemented in OpenCV. The rejection is based on the difference between windows around the feature on the first image and the tracked feature in the second image. If this error is larger than a certain

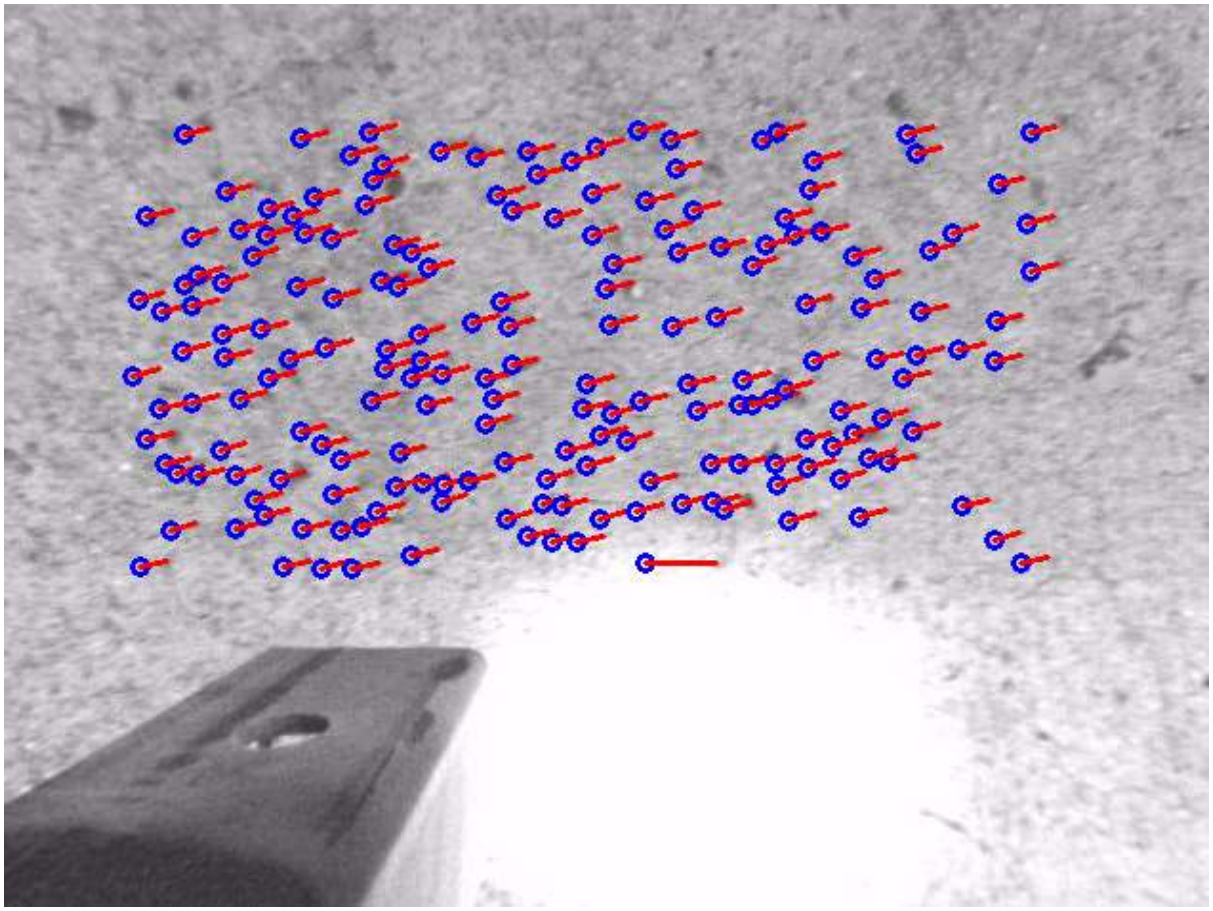

Figure 1 Tracking of corner features with the trace showing the direction of motion.

threshold the feature is rejected. While this method does remove some outliers it fails to remove all outliers, as such another outlier rejection method is employed as well.

The method used is the RANdom SAmple Consesus (RANSAC) algorithm [14], The RANSAC algorithm is an iterative procedure to estimate the parameters of a model from a set of data which is corrupted by outliers. In this simple case the model is simply the direction of travel. The synopsis of the method is to randomly sample a minimum set of data points from which to develop the model, in this only one sample is necessary to estimate the direction of travel. The model is derived from this minimal set and each remaining data point is tested against the model using a suitable metric, in this case the difference in angle. If the error of the metric is below a certain threshold, the data point is considered to agree with the model and counted as an inlier. The process of sampling a minimum set of data points and developing a model continues for a suitable amount of iterations. Upon completion the model with the most inliers is returned as the correct model. In this case rather than use the best model as the correct model, the inliers of the best model is used to average the model over multiple

samples. This algorithm thus allows the model to be based on average value of inliers only. The result of the outlier rejection is shown in Figure 2 showing some tracked features to be regarded as outliers.

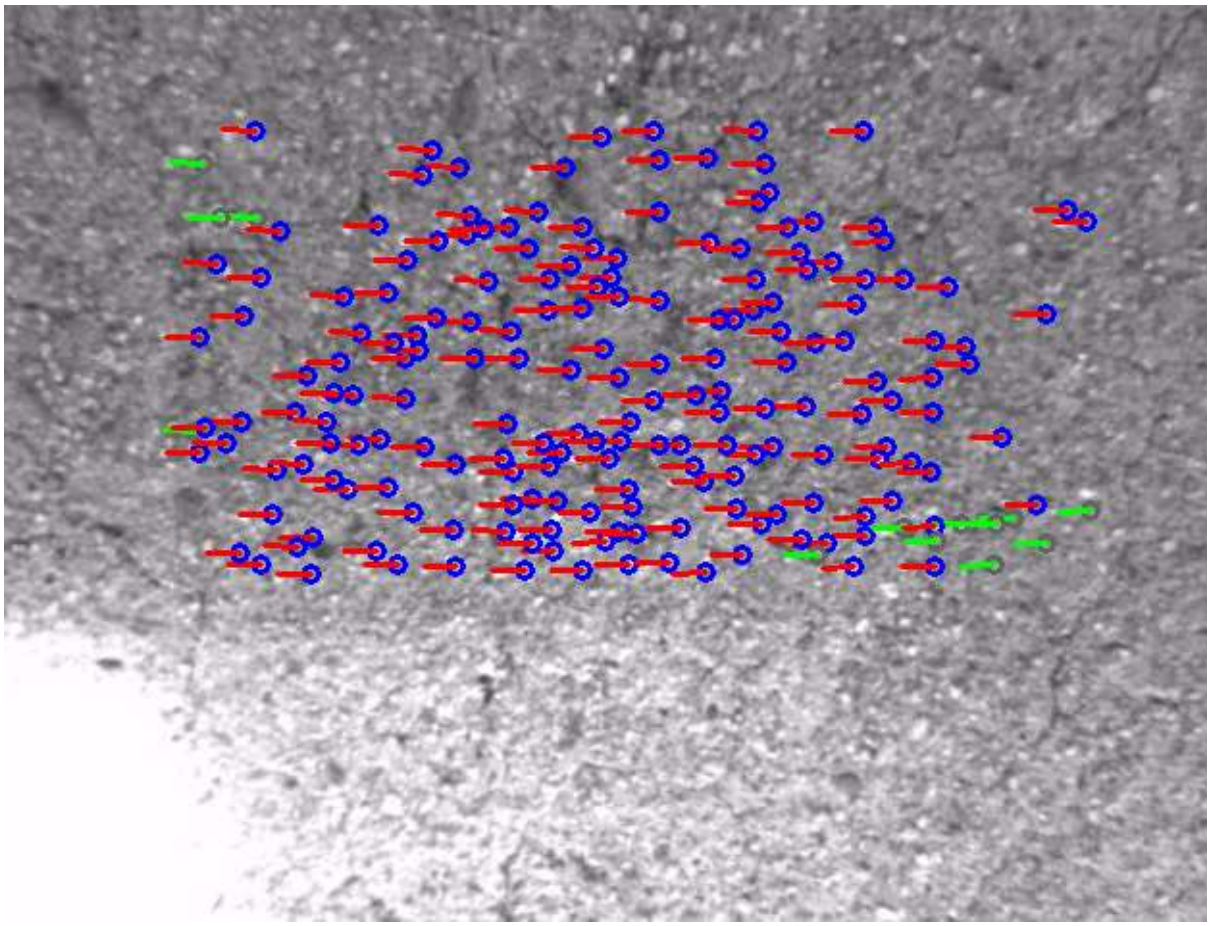

Figure 2 Feature tracking and outlier rejection (red particles are inliers and green are outliers) for the planar method.

This algorithm, which uses only one camera, is computationally inexpensive and can easily be implemented on an embedded system to provide a system that can output an analogue slip angle value in real time. The embedded system need not require much to be capable of providing real time outputs at 500Hz.

3.2. SLIP ANGLE MEASURMENT USING POSE ESTIMATION FROM IMAGE CORRESPONDENCES

The algorithm described above is very basic and can easily be implemented in real time. However, the largest problem with this model is that it assumes only planar motion. While this assumption is valid under traditional paved road conditions the assumption breaks down when considering off-road terrain, which may

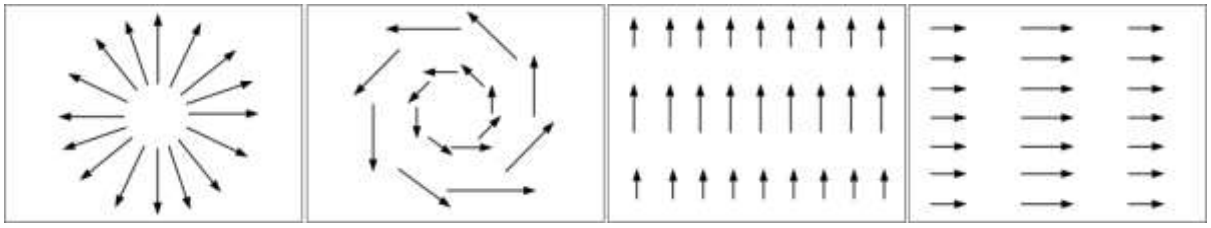

Figure 3 Projected motion onto camera sensor for: a) vertical motion b) yaw motion c) roll motion d) pitch motion of a planar object.

induce vertical motion as well as rotational motions. The effect of these motions on the feature motion which are re-projected onto the camera image is illustrated in Figure 3. This figure shows that motions other than planar may create an ambiguity in measuring the lateral and longitudinal motion. The figure shows the induced motion if it assumed that the camera centre is the centre of rotation, this may not necessarily be the case especially if the camera is not mounted close to the Centre of Gravity (CG) of the vehicle. If the camera is mounted away from the CG certain motions may have a lesser effect, such as the yaw rate. However, mounting the sensor further away from the CG will result in the other rotations, pitch and roll, inducing longitudinal, lateral and vertical motion in the senor. It may be very difficult to differentiate between the motion caused by these effects and actual vehicle motion. It is therefore recommended to mount the sensor close to the CG to reduce these effects when traversing over rough roads. This however still requires the compensation of the other motions in order to determine the direction of travel in the horizontal plane.

To take all of these motions into account requires the implementation of pose estimation algorithms using image correspondences. The problem of estimating relative pose from multiple view-points of scene features has been studied for a long time, initially for photogrammetric purposes and more recently for computer vision. From a mathematical viewpoint the Fundamental matrix $\boldsymbol{F}$ describes the relative projection between two un-calibrated viewpoints.

$$\boldsymbol{F} = \boldsymbol{K}_2^{-1^T}[\boldsymbol{t}]_x \boldsymbol{R} \boldsymbol{K}_1^{-1} \tag{2}$$

Where $\boldsymbol{F}$ is the (3x3) fundamental matrix, $\boldsymbol{K_1}$ and $\boldsymbol{K_2}$ are the calibration matrix from viewpoint 1 and 2 respectively, $\boldsymbol{R}$ is the relative orientation between the two views and $[\boldsymbol{t}]_x$ is the skew symmetric matrix containing the relative translations:

$$[\boldsymbol{t}]_x = \begin{bmatrix} 0 & -t_3 & t_2 \\ t_3 & 0 & -t_1 \\ -t_2 & t_1 & 0 \end{bmatrix} \tag{3}$$

The fundamental matrix also encodes the epipolar constraints between the projections of a real world coordinate onto the two camera image coordinates. The epipolar constraints describes the relation of these images to one another viewing the same scene. The constraint is described as:

$$\boldsymbol{p}'^T \boldsymbol{F} \boldsymbol{p} = 0 \tag{4}$$

The epipolar constrained is depicted in Figure 4 and shows that a point on one camera or view can be represented as a line on the other camera or view.

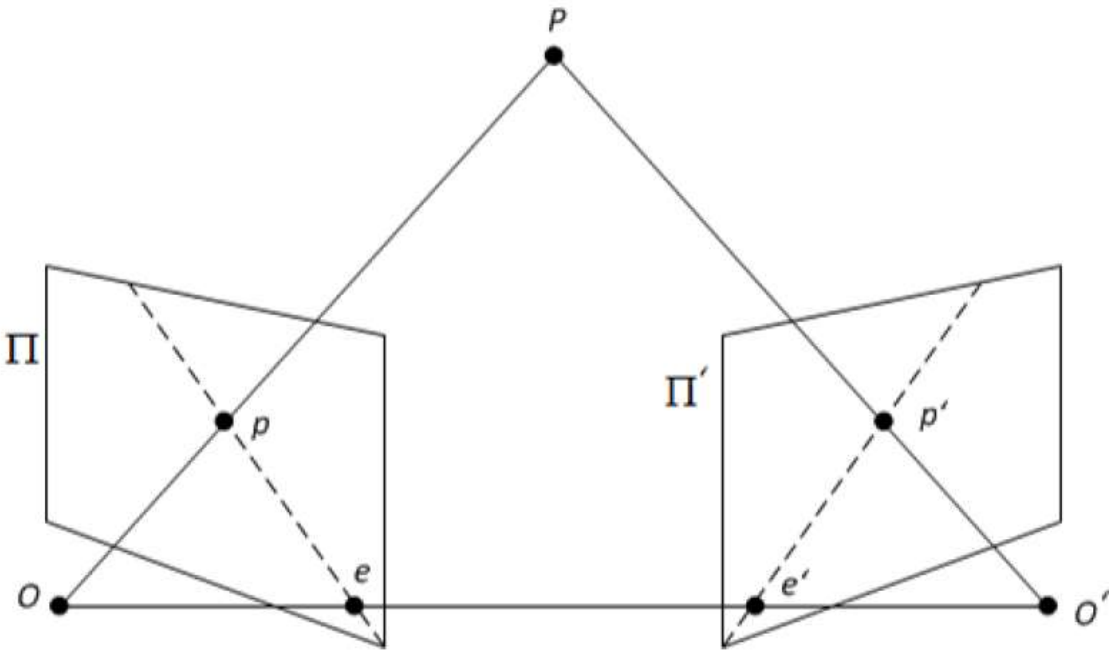

Figure 4 Epipolar constraint of two view system

Where $\boldsymbol{p}$ and $\boldsymbol{p}'$ are point correspondences described in homogeneous coordinates of an object in the first and second images respectively. The homogeneous coordinates are a 3 vector coordinate obtained from the image as $\boldsymbol{p} = [u\ v\ 1]$, where u and v are the image coordinates in the x and y-axis respectively. The

homogeneous coordinates system is a coordinate system used to represent projective geometry. The coordinate system not only simplifies the problem of projecting world coordinates onto a plane, such as the image plane, but also introduces a method of representing a point at infinity using finite coordinates. In most cases the calibration matrices of the cameras are performed beforehand using a known planar surface. Since the calibration matrix is constant for one camera over multiple views $\boldsymbol{K_1} = \boldsymbol{K_2}$. The epipolar constraint (3) can be simplified to:

$$\boldsymbol{q'^T E q} = 0 \tag{5}$$

Where E is known as the essential matrix and maps to the translation and rotation motion as:

$$\boldsymbol{E} = [\boldsymbol{t}]_x \boldsymbol{R} \tag{6}$$

The homogeneous image coordinates $\boldsymbol{q}$ and $\boldsymbol{q'}$ are now presented in terms of the normalized coordinates

$$\boldsymbol{q} = \boldsymbol{K_1^{-1} p} \text{ and } \boldsymbol{q'} = \boldsymbol{K_2^{-1} p'} \tag{7}$$

The remainder of this section focuses on the estimation of the essential matrix from point correspondences. The essential matrix is estimated using multiple correspondences from the two viewpoints. The first method introduced required 8 point correspondences and is therefore termed the 8-point linear algorithm introduced by Longuet-Higgins [15]. While the 8-point algorithm is simplistic in nature it is unfortunately very sensitive to noise in the correspondences. Consequently many alternative algorithms have been developed to estimate the essential matrix and while these algorithms are exceedingly more complex they generally provide superior robustness in the presence of noise [16]. These algorithms also require less correspondences, however, generally produce more than one candidate solutions to the essential matrix. Especially of interest is the 5-point algorithm developed by Stewenius et al [17]. This algorithm is not only robust in the presence of noise, it has also been observed that it is stable if the correspondences are obtained from coplanar objects. Since the terrain which the vehicle is driven across is most likely coplanar or near coplanar, especially when the road is flat, the 5-point algorithm is chosen for estimating the essential matrix. The first step in the algorithm is to use the epipolar constraint (5), the constraint is employed as follows:

$$\begin{aligned} \boldsymbol{q'Eq} &= 0 \\ \widetilde{\boldsymbol{q}}^T \widetilde{\boldsymbol{E}} &= 0 \end{aligned} \tag{8}$$

(9)

Where

$$\tilde{\boldsymbol{q}} = [q_1 q_1' \;\; q_2 q_1' \;\; q_3 q_1' \;\; q_1 q_2' \;\; q_2 q_2' \;\; q_3 q_2' \;\; q_1 q_3' \; q_2 q_3' \;\; q_3 q_3']^T \tag{10}$$

$$\tilde{\boldsymbol{E}} = [E_{11} \;\; E_{12} \;\; E_{13} \;\; E_{21} \; E_{22} \; E_{23} \;\; E_{31} \;\; E_{32} \; E_{33}]^T \tag{11}$$

The vector $\tilde{\boldsymbol{q}}$ is shown for one point correspondence, by using five correspondences a 5x9 matrix build-up of different $\tilde{\boldsymbol{q}}$ vectors is obtained. The Singular Value Decomposition (SVD) algorithm can then be used to obtain the 4 null vectors of the matrix [18]. The 4 vectors of size 1x9 can then be written in a 3x3 matrix form, obtaining matrices $\boldsymbol{E_1}$, $\boldsymbol{E_2}$, $\boldsymbol{E}_3$, $\boldsymbol{E}_4$. The essential matrix is then given by:

$$\boldsymbol{E} = x\boldsymbol{E}_1 + y\boldsymbol{E}_2 + z\boldsymbol{E}_3 + w\boldsymbol{E}_4 \tag{12}$$

where x, y, z, w are scalar values. It is generally assumed that $w = 1$ since the scalar values are only defined up to a common scale factor. This then requires the solution of the remaining scalar values using the trace and determinate constraints. The solution is obtained from solving a multivariate polynomial equation, generally obtained using the Grobner basis method. The method is quite arduous and thus the detail of the solution is omitted here, for detailed descriptions see Stewenius *et al* [17] or alternative method by Nister [19].

The 5-point algorithm can return up to 10 real solutions all of which are candidate solutions to the essential matrix. To obtain the best essential matrix the RANSAC algorithm is employed. A random subset of the minimum number of correspondences is drawn and the 5-point algorithm is used to solve for up to 10 plausible solutions. Each solution is then checked for inliers among the remaining correspondences. The metric used to determine whether a sample is an inlier is the first order geometric distance (Sampson-distance) given as:

$$d_{sampson} = \frac{(\boldsymbol{q}'^T \boldsymbol{E}\boldsymbol{q})^2}{(\boldsymbol{E}\boldsymbol{q})_1^2 + (\boldsymbol{E}\boldsymbol{q})_2^2 + (\boldsymbol{E}^T\boldsymbol{q}')_1^2 + (\boldsymbol{E}^T\boldsymbol{q}')_2^2} \tag{13}$$

where $(\boldsymbol{E}\boldsymbol{q})_i$ is the i[th] entry in the vector $\boldsymbol{E}\boldsymbol{q}$. Another test conducted to determine if the essential matrix is indeed the true essential matrix is that of the cheirality test. The cheirality test is a test which enforces the constraint that the points being imaged should lie in front of both cameras or views. This test first requires

extracting the relative orientation and translation between the frames from the essential matrix. This is accomplished from the thereom given by Tsai and Huang [20]. The solution is obtained by using the singular value decomposition on the essential matrix. It should be noted that four possible solutions are obtained from this procedure:

$$\boldsymbol{E} = \boldsymbol{U} diag(1,1,0) \boldsymbol{V}^T \tag{14}$$

$$\boldsymbol{D} = \begin{bmatrix} 0 & -1 & 0 \\ 1 & 0 & 0 \\ 0 & 0 & 1 \end{bmatrix} \tag{15}$$

$$\boldsymbol{R_a} = \boldsymbol{U}\boldsymbol{D}\boldsymbol{V}^T \tag{16}$$

$$\boldsymbol{R_b} = \boldsymbol{U}\boldsymbol{D}^T\boldsymbol{V}^T \tag{17}$$

$$\boldsymbol{T_a} = [u_{13} \quad u_{23} \quad u_{33}]^T \tag{18}$$

Where matrices $\boldsymbol{U}$ and $\boldsymbol{V}^T$ are the matrices obtained from the singular value decomposition. Two possible rotation matrices $\boldsymbol{R_a}$ and $\boldsymbol{R_b}$ are obtained along with the two possible translation matrices $\boldsymbol{T_a}$ and $\boldsymbol{T_b}$. Any combination of rotation and translation matrix satisfies the epipolar constraints and is thus a possible solution, yielding four possible solutions of which only one is correct. One of the other solutions corresponds to the twisted pair which is obtained by rotating one of the views by 180 degrees. The remaining two solutions correspond to reflections of the true configuration and its twisted pair.

To remove the ambiguity of the motions solutions the cheirality of all four possible solution are tested. This is accomplished by triangulating [21] the five correspondences used to obtain the essential matrix from which these motions are obtained. The triangulation performs a back projection from the two camera images to obtain the scaled world coordinates of each correspondence. The world coordinate is then tested to see whether it lies in front of both cameras or behind any of the cameras. The true configuration should require all five correspondences to be in front of both cameras. Therefore, the solution which contains all five point correspondences in front of the camera is selected as the true motion.

Rodenhorst [16] advises that for efficiency consideration that the cheirality and Sampson-distance inlier test not be conducted on each possible essential matrix. Thus, the cheirality of each real solution from (12) is tested, first. Only candidate essential matrices which have passed the cheirality test, those with all five correspondences

in front of both views, are passed on for further analysis wher the amount of inliers are tested. This methodology, provided that enough RANSAC iterations and enough correct correspondences are present, should result in the correct solution to the essential matrix. From the Essential matrix the relative rotation and translation can be extracted from (14)-(18).

To improve accuracy and allow for triangulation requires that the camera has undergone some translational motion between the two views under consideration. In order to guarantee this, the magnitude of translation, in pixels, is calculated directly from the point correspondences using a RANSAC approach. This ensures that enough motion is present before estimating the essential matrix.

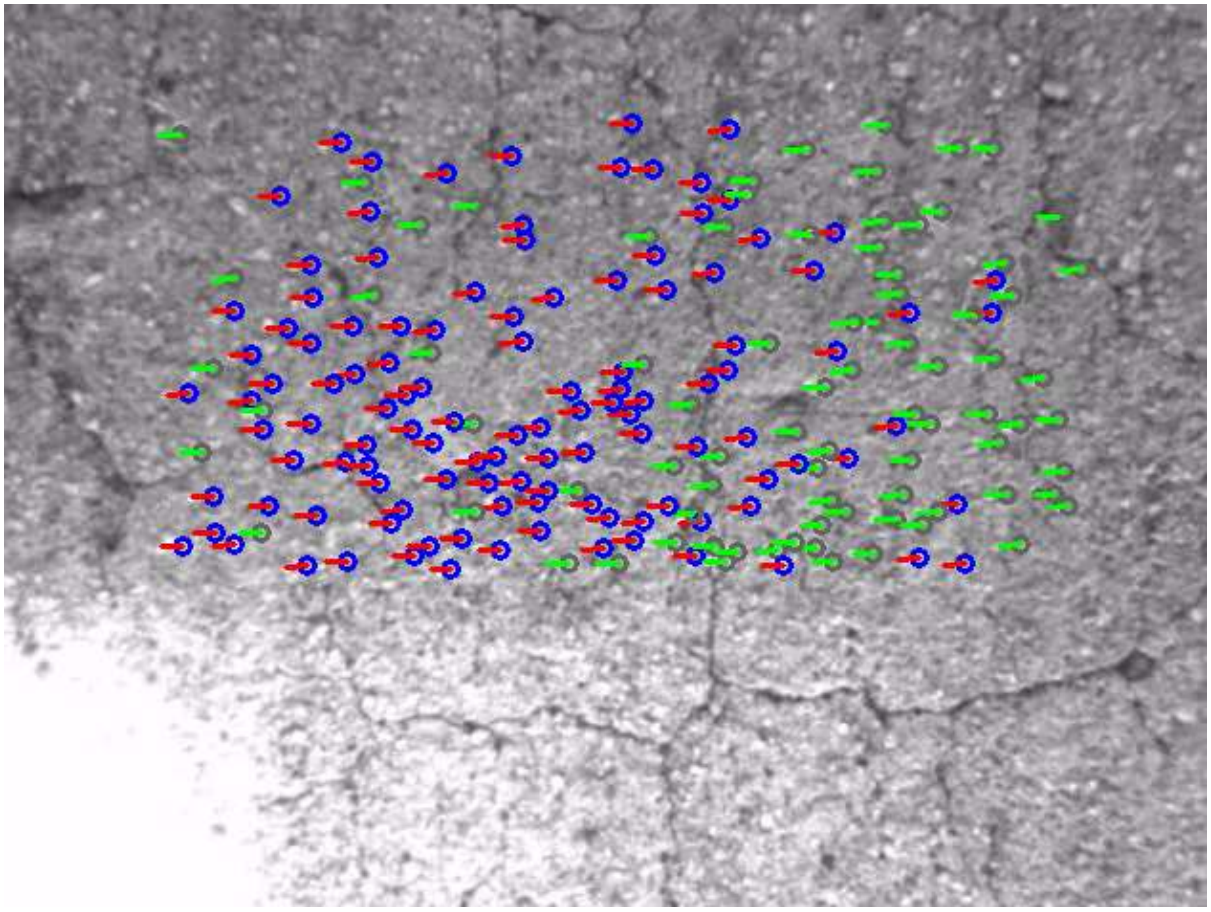

Figure 5 Feature tracking and outlier rejection (red particles are inliers and green are outliers) for the pose method.

The outlier rejection of the pose method is shown in Figure 5, the figure shows that the system classifies more correspondences as outliers compared to the planar method. This is partly due to the enforcement of a stricter inlier threshold to improve the final model. If the translation between frames is less than a certain

threshold, no computation is performed and the frame $\boldsymbol{I_{t+1}}$ is iterated to $\boldsymbol{I_{t+2}}$, without advancing frame $\boldsymbol{I_t}$. This effectively means that the side-slip angle is computed between frames $\boldsymbol{I_t}$ and $\boldsymbol{I_{t+2}}$, producing a variable frequency sampling strategy to ensure that the motion remains above a certain threshold.

This algorithm thus not only provides the slip angle which can be extracted from the longitudinal and lateral motion, but also the vertical velocity as well as all three rotation velocities from a single camera. These additional measurements can be used to evaluate the produced slip angle to ensure that it a result of the vehicle motion rather than the senor motion. The algorithm however requires that a computationally expensive algorithm be performed numerous times per measurement. This makes the methodology difficult to implement in real-time.

3.3. SLIP ANGLE MEASURMENT USING STEREOGRPAHICAL SYSTEM

The pose based system described above has the advantage that it can obtain all translation motions in scale as well as all rotational motions. However, the algorithm is both computationally expensive and the translation motion is obtained in scale and the scale is dependent on the relative motion and is thus not consistent. Therefore another method is proposed which obtains all measurement in real world unscaled coordinates. The algorithm is also capable of real time performance with special hardware. The method uses two cameras to view the same scene at the same time. It therefore allows for 3D measurements much like one of the ways human eyes determines 3D depth. The fundamentals are very similar to that of the pose problem, however, since the cameras are rigidly constrained relative to one another the two cameras can be calibrated using a known calibration surface. The calibration is therefore constant and allows for easy 3D measurements to be obtained. The main problem of the stereographical systems to solve is to determine the disparity of the view. This is to say the relative image distance between features in the left and right views. The image disparity can then be mapped to depth by using a calibration matrix obtained during initial calibration of the rig.The disparity can be obtained similarly to DIC described above which is used to track movement between two views. However, alternative algorithms are available which are highly parallel and obtain a full 3D view across most of the image.

There are various algorithms used to determine the disparity from two images. One of the most basic and computationally inexpensive algorithms is the so called block matching algorithm [22]. The block matching algorithm computes disparity by means of a suitable metric. The most common metric is the Sum of Absolute Differences (SAD) of a moving window (*NxN* window). The disparity of a pixel in the left image is determined by matching the surrounding pixel region to regions in the right image. The disparity is obtained from the region

providing the best match. To simplify the search one can use the epipolar geometry of the cameras to transform the image in such a manner that the epipolar lines are horizontal. This results in any feature in the left transformed image to lie on the same horizontal line on the transformed right image. The calibration is performed by means of a planar calibration surface which has dots in known positions. Multiple images of the calibrations surface are taken in different orientations and positions with both cameras. The positions of these dots are used to obtain the relative position and orientation between the two cameras. The relative positions and orientations are used in the stereo calibration to be able to realign the images such that the Epipolar lines run horizontally to ease the stereo correspondence. The calibrations surface is also used to correct for lens distortion. The realignment of the images simplifies the stereo correspondence to perform simple line searches instead of an exhaustive search over the entire image. The SAD metric is defined as:

$$SAD = \sum_{i=-N/2}^{N/2} \sum_{j=-N/2}^{N/2} |I_L(x+i, y+j) - I_R(x+i+d, y+j)| \tag{20}$$

where N is the window size and d is the disparity. In some algorithms additional heuristic methods are applied to improve correspondence matching. As required by the motion tracking it is required that the surface has some arbitrary features which create luminosity variations across the images. The luminosity variations can be used to differentiate regions from one another, thus monotone surfaces may be very difficult to apply this technique to. However, as demonstrated most roads have arbitrary features such as grooves, stones and other discolouration which identify unique regions. More complex techniques with multiple variations, as well as pre and post filtering to improve disparity estimation, are also available. However, the block matching technique is chosen due to its simplicity and fast solving time while still providing decent a estimation of disparity. The Open Computer Vision (OpenCV) library [23] is used for calibration and disparity estimation.

Once a 3D map has been generated from the two cameras, features can be tracked in the left image using the technique mentioned earlier. Since the disparity and therefore 3D coordinates are performed relative to the left image the 2D pixel coordinates from the tracking process can easily be transformed into 3D real world coordinates. This is to say that the coordinates of the points are provided in units such as millimetres relative to the camera origin instead of pixels. This yields several 3D points in space which have undergone rigid motion between two views of which the position is known in both views. The relative translation and rotation can then be determined provided at least three point correspondences have been obtained [24]. The problem being solved is the rotation matrix $\boldsymbol{R}$ and translation vector $\boldsymbol{t}$ in:

$$\boldsymbol{P_2} = \boldsymbol{R}\boldsymbol{P_1} + \boldsymbol{t} \tag{21}$$

Where the N 3D points set $\boldsymbol{P_1}$ undergoes rigid motion to yield the points set $\boldsymbol{P_2}$. The method starts of by finding the centres of $\boldsymbol{P_1}$ and $\boldsymbol{P_2}$:

$$\overline{\boldsymbol{P_1}} = \frac{1}{N}\sum_{i=1}^{N} \boldsymbol{P_1^i} \tag{22}$$

where $\boldsymbol{P_1^i}$ is the i^{th} 3D point correspondence. Next the covariance matrix between points set $\boldsymbol{P_1}$ and $\boldsymbol{P_2}$ are determined as:

$$\boldsymbol{\Sigma} = \sum_{i=1}^{N} \left(\boldsymbol{P_1^i} - \overline{\boldsymbol{P_1}}\right)\left(\boldsymbol{P_2^i} - \overline{\boldsymbol{P_2}}\right)^T \tag{23}$$

The rotation matrix $\boldsymbol{R}$ is obtained from the Singular Value Decomposition (SVD) of the covariance matrix:

$$\boldsymbol{\Sigma} = \boldsymbol{U}\boldsymbol{S}\boldsymbol{V}^T \tag{24}$$

$$\boldsymbol{R} = \boldsymbol{V}\boldsymbol{U}^T \tag{25}$$

If the determinate of $\boldsymbol{R}$ is negative the solution corresponds to an inflection, the rotation matrix is then recalculated as:

$$\boldsymbol{R} = \boldsymbol{V}\begin{bmatrix} 1 & 0 & 0 \\ 0 & 1 & 0 \\ 0 & 0 & -1 \end{bmatrix}\boldsymbol{U}^T \tag{26}$$

The translation vector is the obtained from:

$$\boldsymbol{t} = \overline{\boldsymbol{P_2}} - \boldsymbol{R}\overline{\boldsymbol{P_1}} \tag{27}$$

While this method requires at least 3 point correspondences, the method will calculate the rotation and translation in a least mean square sense for any point sets with N correspondences. Thus, several point correspondences (≈ 50) are used to obtain the average motion between frames. However, to prevent any outliers from influencing the calculation of the rotation and translation the RANSAC algorithm is used to remove outliers. The model is derived from 3 randomly drawn point correspondences. The remaining data set is tested against the derived model for inliers using the following error metric, $\epsilon = \left\|\boldsymbol{P_2^i} - (\boldsymbol{R}\boldsymbol{P_1^i} + \boldsymbol{t})\right\|$. Upon completion the model with the most inliers is returned along with the set of inliers. The rotation and translation

is then determined in a least square sense using all of the inliers of the best model. Figure 6 shows the tracked features on a colour depth map of the surface as well the corresponding original left camera image.

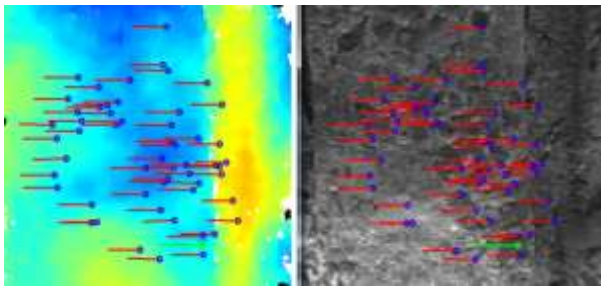

Figure 6 Feature tracking and outlier rejection (red particles are inliers and green are outliers) for the stereographic rig in the depth colour (left) map and right on the original image (right)

This yields a system whereby all translations and rotations can be obtained unscaled in real world coordinates using a two camera system. The most computationally expensive part of the algorithm is the disparity mapping. However, using Field Programmable Gate Array (FPGA) has yielded systems capable of performing the disparity mapping using more advanced algorithms at over 500fps [25]. Thus, this system is capable of yielding a system capable of real time performance at over 500fps.

All camera based systems include a form of variable frequency sampling method to improve measurement accuracy at low speeds. The methodology works by determining the distance travelled from the previous frame using a RANSAC approach. In the single camera methods the distance is determined in pixels and in the stereographic rig the distance can be set to real world units such as millimetres. If the distance travelled is below a threshold then the previous frame is not advanced to the current frame in the next sample. The current frame is still advanced on the next sample, therefore the calculation is now performed with a larger frame difference. This processes is repeated either until the distance travelled is above a threshold or the frame difference is above a threshold. This therefore creates a form of variable sample frequency sampling method without changing the camera sample frequency.

3.4. CAMERA AND LENS SPECIFICATIONS

It should be noted that the camera and lens specification can affect the accuracy and speed at which the system works reliably. The camera specifications which will have the most effect are the resolution, frame rate and shutter opening time. An increased resolution will increase the accuracy of the measurements but will reduce the maximum frame rate the cameras can achieve therefore affecting the maximum speed at which the

systems works. The maximum speed attainable by the system is related to camera speed which will allow a sufficient overlap of the images and the shutter time of the cameras to allow images which are not blurred.

The lens can also affect the accuracy and the maximum operating speed dependent on the focal length of the lens. A small focal length can be used to enlarge the area in view which would allow the system to be operated at higher speeds. A larger focal length can be used to improve accuracy by imaging a smaller area making it more sensitive to smaller motions.

The selection of the camera and lens is dependent on what is most desirable. If low speed accuracy is preferred then higher resolution camera and larger focal length lenses can be used. If the requirement is high speed measurement then higher sampling frequency and smaller focal length lenses are used. If both are desired then either a compromise is needed or a variable focal length, variable resolution system can be used to switch between the low speed and high speed.

4. EXPERIMENTAL TESTS

In order to validate the results of the algorithms, tests were performed on both smooth roads as well as off-road terrain. The setup consisted of a calibrated stereographic camera rig. The cameras are Point Grey Flea3 USB 3 cameras with maximum resolution of 1280 x 1024 and a global shutter. The lens is a Kowa 4mm focal length c-mount lens. The lens is a wide angle lens providing a large image area even when mounted close to the ground. The cameras are set to resolution 640x480 at which a maximum of 600fps can be obtained per camera. The cameras are mounted next to a Corrsys-Datron Correvit S-HR slip angle sensor viewing the same region of road and sampling at 250fps. The sensors were synchronised using a synchronising pulse, generated by the data acquisition device.

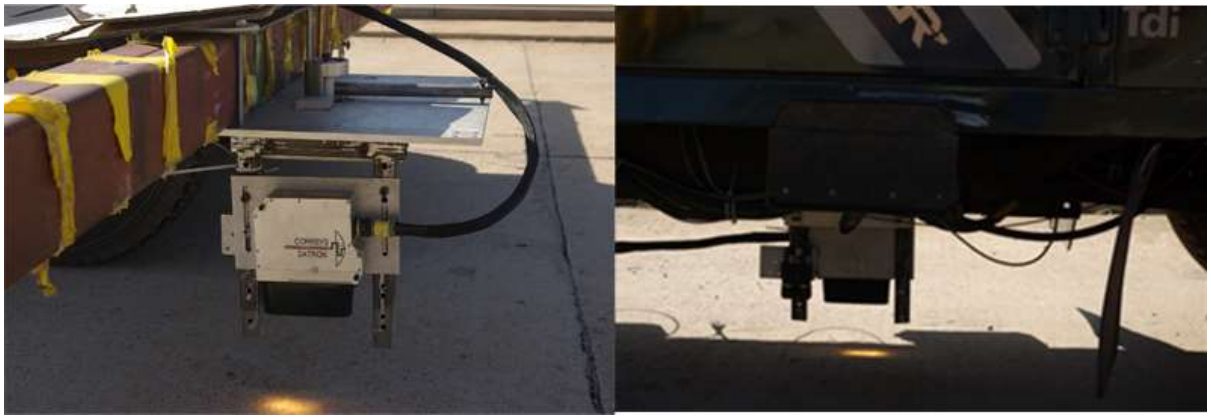

Figure 7 Test setup showing two cameras and Corrsys-Datron S-HR slip angle sensor

To validate the measurements both sensors were mounted on a gimbal which allowed the sensors to be rotated in one degree increments relative to the vehicle as shown in Figure 7. This allows for the side-slip angle to be set at a constant angle while the vehicle moves in a straight line. The gimbal system is mounted underneath the vehicle as close as possible to the CG of the vehicle to reduce the effect of the roll and pitch motions. The slip angle was set to 0, 2, 5 and 10 degrees whilst driving over both a flat surface and a rough Belgian paving surface at Gerotek Test Facilities [26].

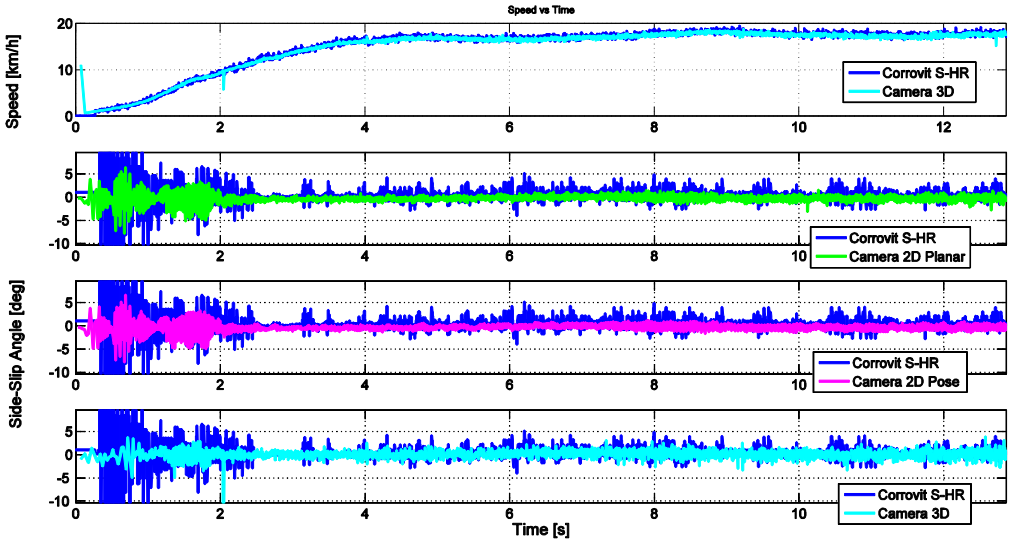

Figure 8 Vehicle speed and side-slip angle comparison between camera based techniques and Corrsys-Datron Correvit S-HR side-slip angle sensor on flat surface for zero degrees slip angle.

The vehicle speed and side-slip angle for all sensors and algorithms driving over a flat surface with the gimbal set at a side-slip angle of 0 degrees is shown in Figure 8. Each algorithm is individually compared to the Correvit S-HR slip angle sensor. It can be noted that the Correvit S-HR sensor has a larger noise band than the other measurements especially at lower speeds. The Correvit S-HR only provides decent accuracy at speeds over 10-15km/h, even then the noise band is not consistent. At best the noise levels are comparable to the measurements obtained from the camera based measurements and at worst almost an order of magnitude worse. The camera based systems have better noise bands at lower speeds with the 3D system having the smallest noise band at very low speeds. The improved accuracy at low speeds can be partially attributed to the variable frequency sampling method employed which increases the distance between points used to determine the slip-angle and therefore improves accuracy. All measurements also increase in accuracy as vehicle speeds increase. The vehicle speed obtained from the 3D method also compares exceptionally well to that of the velocity of the

Correvit S-HR sensor. The vehicle speed can also be obtained from the 2D planar algorithms however the measurement is scaled, therefore if the vehicle height remains constant the scale will be the same. However, since the height of the sensor may change the measurement of the method is not reliable. The vehicle speed obtained from the 3D algorithm is obtained using real world coordinates and is therefore independent of sensor height. The noise band of the velocity from the 3D algorithm is also smaller compared to the Correvit S-HR sensor. No noticeable difference can be ascertained between the different camera based measurements. Figure 9 shows some of the other motions measured by the pose and 3D algorithms. These measurements show no discernible motions as expected as the vehicle is traveling over a smooth surface.

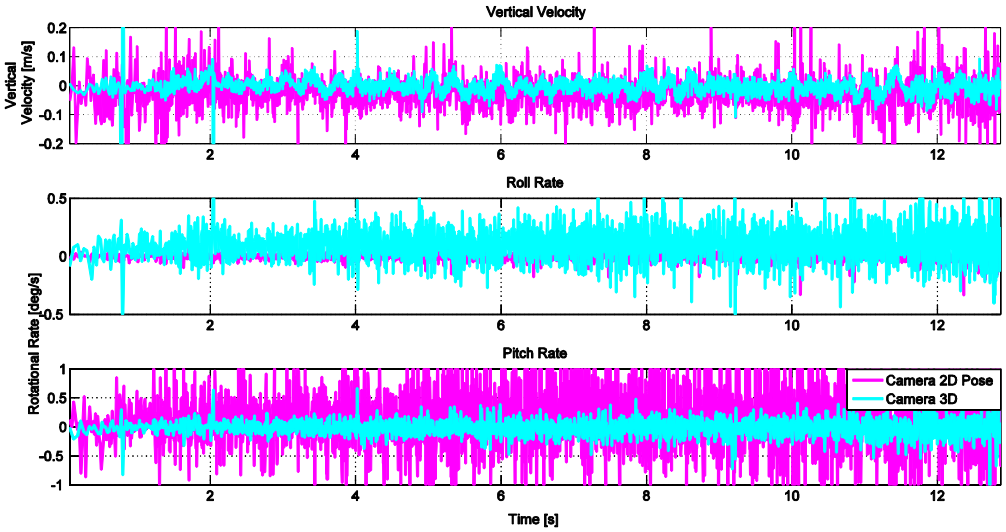

Figure 9 Vertical velocity, roll and pitch rate from 2D pose and 3D camera based methods, on flat surface for zero slip angle.

Figure 10 depicts the speed and side-slip angle for all sensors and algorithms driving over a Belgian paving surface with the side-slip angle set at 10 degrees. Similar tendencies on the Belgian paving as the flat surface can be observed. These tendencies include a smaller noise band at lower speeds as well as a smaller noise band overall for the camera based systems as compared to the Correvit S-HR sensor. Figure 11 shows the vertical velocity, roll rate and pitch rate from the 2D pose method and 3D method. The vertical velocity from the 2D pose method is scaled such that the magnitudes appear to be the same. From these plots it is clear that there is a change in vertical velocity which appears oscillatory, however, the roll and pitch rate show no discernible trend or oscillations. The vertical velocity of the 2D pose method appears to contain considerably more noise than the 3D method. This is mostly due to inconsistent scale of 2D pose method which makes it seem noisy. The 3D

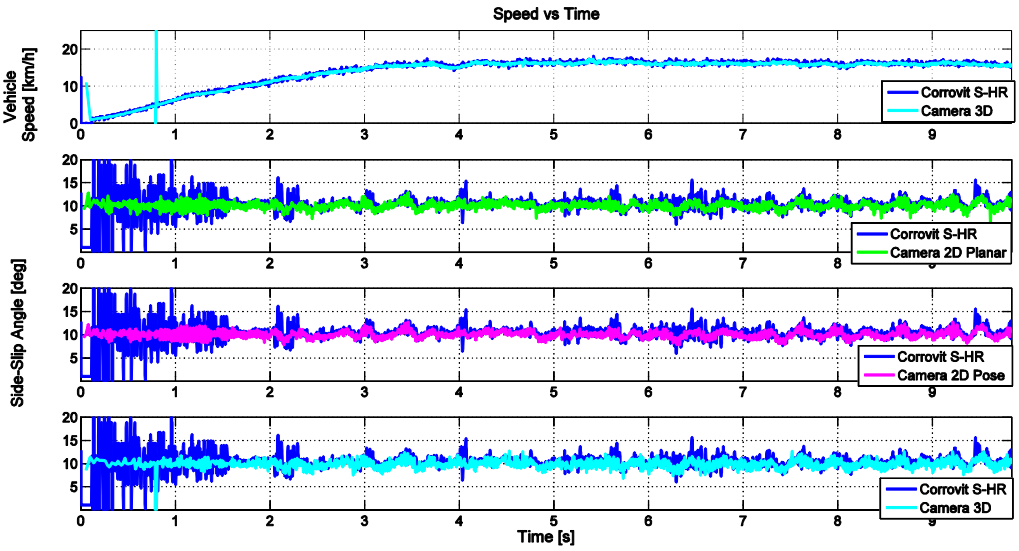

Figure 10 Vehicle speed and side-slip angle comparison between the camera based techniques and Corrsys-Datron Correvit S-HR side-slip angle sensor on Belgian paving surface for 10 degrees slip angle.

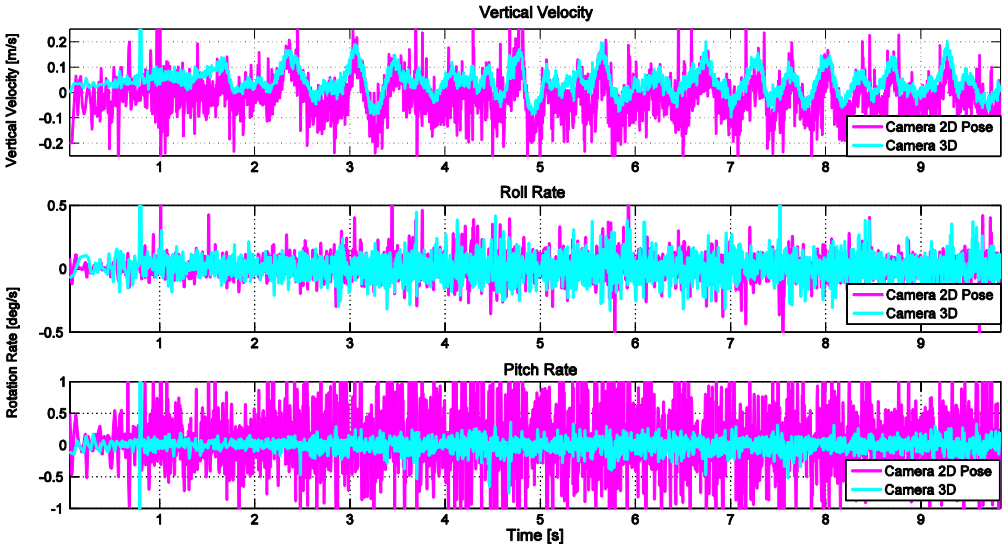

Figure 11 Vertical velocity, roll and pitch rate from 2D pose and 3D camera based methods, on flat surface for zero slip angle.

method however contains a much cleaner vertical velocity measurement. A zoomed in section is displayed in Figure 12 comparing all methods against one another. The figure shows that all camera methods appear to provide the same measurements irrespective of whether they take into consideration other motions. The side-slip angle however still appears to be oscillatory even though the vehicle maintains a straight driving line. The oscillatory nature is still likely caused by other vehicle motions. However, the motions most likely cause the slip angle sensor to move relative to the ground as the vehicle body moves. This results in a side-slip angle to be

generated at the sensor which is not necessarily caused by the side-slip angle of the vehicle. To further investigate this, a Power Spectral Density of both the side-slip angle and the vertical velocity is shown in Figure 12. The plot indicates that both measurements have high energy content at the same low frequencies. This indicates that the vertical velocity could be the effect which causes the oscillatory nature in the side-slip angle.

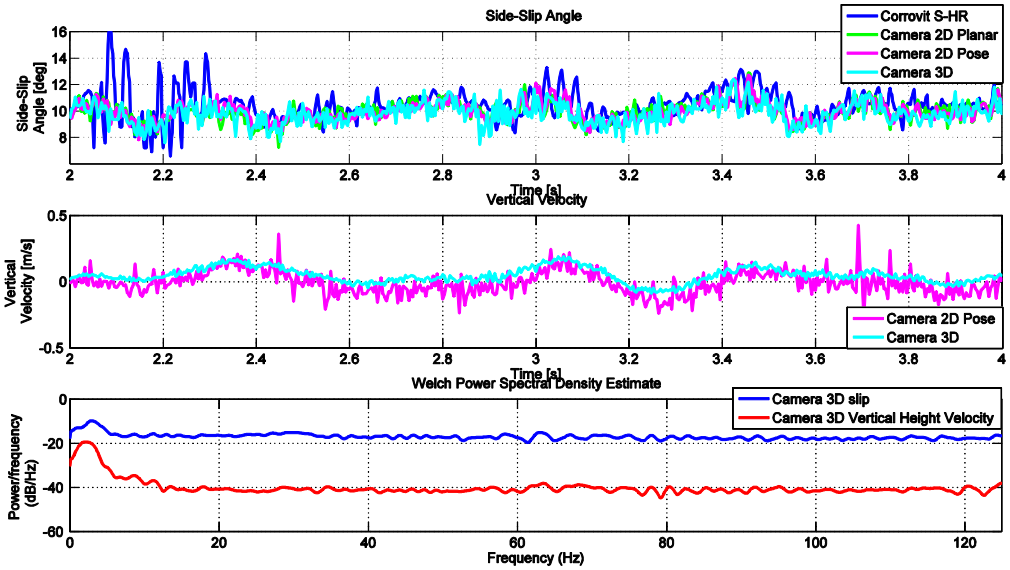

Figure 12 Enlarged region comparing different side-slip angle techniques, vertical velocity and power spectral density of 3D camera method side-slip angle and vertical velocity.

Another experiment conducted was to move the mounting point of the sensors further away from the CG to near one of the wheels. The reason for this mounting position is that it is often easier to mount the sensors at this location as compared to the CG where space and ground clearance may be an issue. The side-slip angle of the tyres is also often measured to conduct tyre lateral force characterisation. The vehicle was driven in a straight line over the Belgian paving as in the previous test. Figure 13 shows a comparison of the side-slip angle at the different mounting positions with the slip angle set at 5 degrees, the measurements are obtained using the 2D pose algorithm. The figure clearly shows that the measurements at the wheel have much larger oscillations compared to the measurements at the CG. The vertical velocity also shows much larger values, however, it should be noted that the scale may not exactly be identical. This indicates that the reduction of the other vehicle motions improves the accuracy of the measured side-slip angle. The effect these motions have on the sensor should also be reduced by mounting the sensor as close to the vehicle CG as possible.

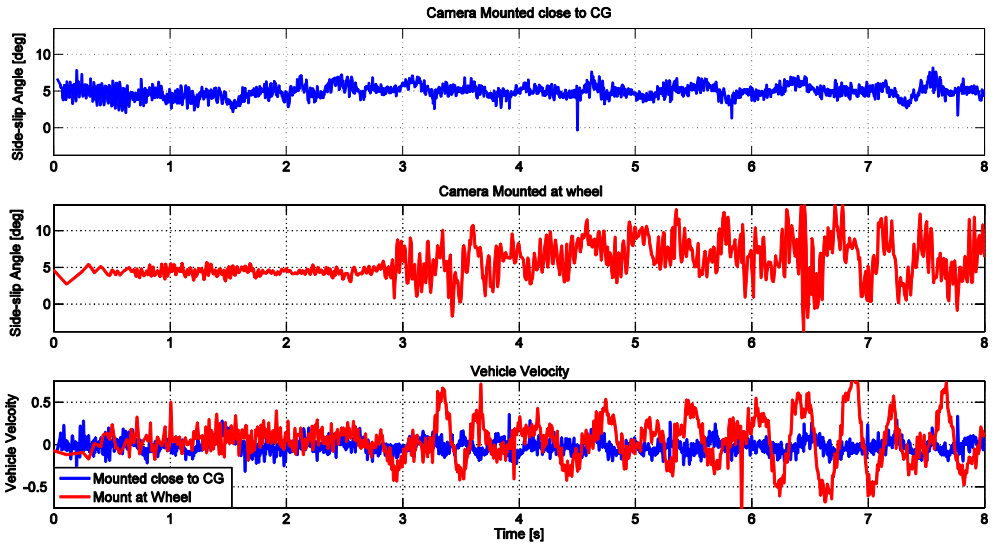

Figure 13 Comparison between side-slip angle and vertical velocity at the CG and wheel mounting locations.

The remainder of the tests at the other side-slip angles are tabulated in Table 1. The results are presented in RMS values, mean and Standard Deviation (STD). These values indicate how consistently the measurement measures the correct side-slip angle. The results show that the Correvit S-HR has a consistently larger standard deviation and that the mean and RMS values are further away from the correct set point. The results between the camera based measurements are very similar showing no discernible difference between the algorithms.

While the tests were performed on hard terrain the same results can be expected on any terrain provided that there are features on the terrain which can be tracked and that the terrain being viewed does not deform much. The first requirement that the surface contain features is true for most natural surfaces even for sand. The requirement may be invalid on artificial surfaces or wet surfaces. The second requirement will be valid if the measurement is not performed at the wheels which may rework the terrain and move the soil. This is not a problem if the measurement is performed at the CG but could represent a problem when performed very close to the wheel. Another aspect could be dust obscuring the surface from view of the cameras. The dust should be so severe to remove all visibility of the surface. Even if the visibility becomes partially reduced there should be enough visibility for the system to track features. Future studies could be conducted to quantify this possible problem.

Tests were also conducted at steady state slip angles due to the ease of comparing the results of all the systems to the set-point. The system can however measure transient slip angles depending on the frame rate of

the cameras. The system should be able to measure frequency events up to half the sampling frequency of the cameras as limited by the nyquist frequency. The phase lag should be at most be one sample since the slip angle is calculated using the movement between two images.

Table 1: RMS, mean and standard deviation for all techniques at various slip angles over a flat and Belgian paving surface.

	Correvit S-HR			2D Planar			2D Pose			3D		
Flat	**RMS**	**Mean**	**STD**	**RMS**	**Mean**	**STD**	**RMS**	**Mean**	**STD**	**RMS**	**Mean**	**STD**
0	2.30	0.42	2.26	0.91	-0.36	0.84	0.91	-0.31	0.85	0.83	0.06	0.83
2	2.76	2.45	1.28	1.87	1.75	0.66	1.89	1.76	0.69	1.81	1.70	0.60
5	5.86	5.48	2.09	4.98	4.90	0.89	5.02	4.92	0.98	4.93	4.85	0.87
10	10.39	10.10	2.45	9.96	9.95	0.53	9.97	9.95	0.60	9.81	9.77	0.87
BELG	**RMS**	**Mean**	**STD**	**RMS**	**Mean**	**STD**	**RMS**	**Mean**	**STD**	**RMS**	**Mean**	**STD**
0	1.71	0.65	1.58	0.91	-0.09	0.91	0.94	-0.02	0.93	0.92	-0.09	0.92
2	2.98	2.52	1.59	2.10	1.85	0.99	2.18	1.92	1.04	2.06	1.83	0.95
5	5.60	5.42	1.42	4.92	4.85	0.83	4.97	4.90	0.86	4.89	4.79	0.96
10	10.56	10.35	2.12	10.03	10.00	0.75	10.07	10.04	0.78	9.90	9.87	0.87

5. CONCLUSION

Three techniques capable of measuring the side-slip angle based on camera images are presented in this paper. Two of the methods use a single inexpesnive camera to measure the side-slip angle. The first method measures the slip using the projected features on the camera image. This method relies mostly on the camera motion being planar. The second method uses a 5 point pose estimation algorithm to estimate the scaled translational and rotational velocities. This pose technique corrects for certain errors induced by other vehicle motion and provides additional information over the planar technique. The third method relies on two inexpensive cameras configured in a calibrated stereographic rig to measure 3D world coordinates. This allows for all translations and rotations to be measured in unscaled real world coordinates. The algorithms are

compared to a Corrsys-Datron Correvit S-HR commercial side-slip angle sensor. Tests were conducted over both a flat surface as well as a Belgian paving surface. The tests show that the camera based techniques have a lower noise band especially at low speeds compared to the Correvit S-HR sensor. The better accuracy can be due to the variable frequency method employed. The accuracy can also be improved by increasing the camera resolution and increasing the focal length which would however reduce the maximum operating speed. No discernible differences between the camera based techniques were observed even over the rough terrain.

However, the pose and 3D algorithm provide more information compared to the Correvit S-HR and 2D planar methods. The 2D planar method can easily be converted into a real time method. The 3D algorithm can also potentially be performed in real time using FPGA's, as studies have shown. The 2D pose method on the other hand is the most computationally intensive algorithm of all three and is therefore currently limited to off-line analysis. It however does not require any additional requirement than the 2D planar method to be performed. If off-line analysis are considered the raw image data can easily be passed through both single camera techniques. The 3D camera technique, while providing better information, has the added complexity of using two cameras. The cameras must be calibrated and have a rigid connection between one another. The images of the cameras should also have similar illumination and should have similar focus points.

If planar motion or small rotational excitation is experienced the planar motion is recommended. However, the 3D or 2D pose methods are recommended if the vehicle experiences larger vehicle excitations, especially if these excitations are large in comparison to the vehicle velocity.

6. NOTATION

$d_{samposn}$	Sampson distance
I_t	Frame at time t
I	Image pixel intensity
$\boldsymbol{E}$	Essential matrix
$\boldsymbol{F}$	Fundamental matrix
$\boldsymbol{K_1}, \boldsymbol{K_2}$	Camera calibration matrices
$\boldsymbol{P_1}$	Point set 1

$\overline{\boldsymbol{P_1}}$	Mean of point set 1
$\boldsymbol{p}$	Homogeneous coordinate of point in image I_t
$\boldsymbol{p'}$	Homogeneous coordinate of point in image I_{t+1}
$\boldsymbol{q}$	Normalised homogeneous coordinate of point in image I_t
$\boldsymbol{q'}$	Normalised homogeneous coordinate of point in image I_{t+1}
$\boldsymbol{R}, \boldsymbol{R_a}, \boldsymbol{R_b}$	Rotation matrices
$\boldsymbol{t}, \boldsymbol{T_a}, \boldsymbol{T_b}$	Translation vectors
$[\boldsymbol{t}]_x$	Skew symmetric translation matrix
t_i	Component *i* from translation vector
$\boldsymbol{U}$	Left SVD singular vector matrix
$\boldsymbol{V}$	Right SVD singular vector matrix
$\boldsymbol{\Sigma}$	Singular values from SVD

ACKNOWLEDGEMENTS

The financial assistance of the National Research Foundation (DAAD-NRF) towards this research is hereby acknowledged. Opinions expressed and conclusions arrived at, are those of the author and are not necessarily to be attributed to the DAAD-NRF.

REFERENCES

[1] Fiala E. Seitenkrafte am rollenden Luftreifen. VDI Zeitschrift. 96, 973; 1954

[2] Bakker E, Nyborg L, Pacejka HB. Tyre modelling for use in vehicle dynamics studies. Conference: Society of Automotive Engineers international congress and expo. 23 Feb 1987. Detroit, MI, USA,

[3] Sandu C, Taylor B, Biggans J, Ahmadian M. Building Infrastructure for Indoor Terramechanics Studies: The Development of a Terramechanics Rig at Virginia Tech. Proceedings of the 16th International Conference of the International Society for Terrain Vehicle Systems (ISTVS), Nov. 25-28, 2008, Turin, Italy.

[4] Krick G. Behavior of Tyres Driven in Soft Ground with Side Slip. Journal of Terramechanics, 1973, Vol. 9, No. 4, pp. 9-30.

[5] Inagaki S. Kshiro I, Yamamoto M. Analysis on vehicle stability in critical cornering using phase-plane method. Proc. Int. Symp. Advanced Vehicle Control. 1994, pp. 287–292.

[6] Chung T, Yi K. Design and Evaluation of Sideslip Angle-Based Vehicle Stability Control Scheme on a Virtual Test Track, IEEE Transactions on Control System Technology, 2006;14:2, pp. 224-234.

[7] Botha TR, Els PS. Vehicle Sideslip Estimation Using Unscented Kalman Filter, AHRS and GPS. Proceedings of the 14th International Conference on Advanced Vehicle and Tire Technologies AVTT14 August 12-15, 2012, Chicago, IL, USA DETC2012-70875.

[8] Bevly DM, Ryu J, Gerdes JC. Integrating INS Sensors With GPS Measurements for continuous Estimation of Vehicle Sideslip, Roll, and Tire Cornering Stiffness. IEEE Transaction on intelligent Transportation System, 2006;7:4, pp. 483-493.

[9] Kistler. Correvit S-HR Sensor. [Viewed 09,09,14 from http://www.kistler.com/us/en/product/velocity/CSHRA22111]

[10] Xavier J, Sousa AMR, Morais JJL, Filipe VMJ, Vaz M. Measuring displacement fields by cross-correlation and a differential technique: experimental validation. Optical Engineering 2012;51:4

[11] Shi J, Tomasi C. Good Features To Track. 9th IEEE Conference on Computer Vision and Pattern Recognition, June 1994.

[12] Lucas BD, Kanade T. An iterative image registration technique with an application to stereo vision. Proceedings of the 1981 DARPA Imaging Understanding Workshop 1981: pp. 121–130.

[13]OpenCV [viewed 10,03,14 from http://opencv.org/]

[14] Fischler MA, Bolles RC. 1981. Random sample consensus: A paradigm for model fitting with applications to image analysis and automated cartography. Communications of the ACM, 1981;24:6, pp. 381–395.

[15] Longuet-Higgins HC. A Computer Algorithm for Reconstructing a Scene From Two Projections. Nature, Sept 1981; 293, pp. 133–135.

[16] Rodehorst V, Heinrichs M, Hellwich O. Evaluation Of Relative Pose Estimation Methods For Multi-Camera Setups. The International Archives of the Photogrammetry, Remote Sensing and Spatial Information Sciences.. 2008; XXXVII. Beijing

[17] Stewenius H, Engels C, Nister D. Recent Developments on Direct Relative Orientation. Journal of Photogrammetry & Remote Sensing 2006;60, pp. 284–294

[18] Khare SR, Pillai HK, Belur MN, Algorithm to Compute Minimal Nullspace Basis of a Polynomial Matrix. Proceedings of the 19th International Symposium on Mathematical Theory of Networks and Systems – MTNS. 2010, 5–9 July, Budapest, Hungary

[19] Nister D. An Efficient Solution to the Five-Point Relative Pose Problem IEEE Transactions On Pattern Analysis And Machine Intelligence. 2004;26:6

[20] Tsai RY, Huang, TS. Uniqueness and Estimation of Three-Dimensional Motion Parameters. IEEE Transactions On Pattern Analysis And Machine Intelligence. 1984;6:1

[21] Hartley RI, Sturm P. Triangulation. Computer Vision And Image Understanding. 1997; 68:2, pp. 146–157,

[22]Konolige K. Small vision systems: hardware and implementation. Eighth International Symposium on Robotics Research. 1997, pp.111–116.

[23] Bradski, G. 2000, The OpenCV Library, Dr. Dobb's Journal of Software Tools.

[24] Arun, K. S., Huang, T. S. and Blostein S. D. 1987. Least-Squares Fitting Of Two 3-D Point Sets IEEE Transactions On Pattern Analysis And Machine Intelligence, Vol. Pami-9, No. 5, September 1987

[25] Georgoulas, C. and Andreadis, I. 2009. A Real-Time Occlusion Aware Hardware Structure for Disparity Map Computation. Image Analysis and Processing – ICIAP 2009 Lecture Notes in Computer Science Volume 5716, 2009, pp 721-730

[26] Gerotek Test Facilities [viewed 08,09,14 from www.gerotek.co.za]